Energy Storage Materials 84 (2026) 104834

Contents lists available at ScienceDirect

Energy Storage Materials

journal homepage: www.elsevier.com/locate/ensm

A coordination-reinforced and encapsulated polymer electrolyte for durable and safe Na-metal batteries

Junhao Chen [a,b,†], Wentao Lin [b,c,†], Zhantao Wu [b], Dengjie Chen [b,**], Ho Mei Law [d,e], Francesco Ciucci [d,e,*], Jing Yu [a,**]

[a] College of Chemical and Materials Engineering, Zhongkai University of Agriculture and Engineering, Guangzhou 510225, China
[b] College of Chemistry and Materials Science, Jinan University, Guangzhou 510632, China
[c] The Hong Kong University of Science and Technology (Guangzhou), Sustainable Energy and Environment Thrust, Guangzhou 511400, China
[d] Chair of Electrode Design for Electrochemical Energy Systems, University of Bayreuth, Bayreuth 95448, Bavaria, Germany
[e] Bavarian Center for Battery Technology (BayBatt), University of Bayreuth, Bayreuth 95448, Bavaria, Germany

ARTICLE INFO

Keywords:
Coordination
Encapsulation
Gel polymer electrolyte
Na-metal batteries
Low-temperature batteries

ABSTRACT

Gel polymer electrolytes are a promising alternative to flammable organic electrolytes for Na-metal batteries. However, their utilization is hindered by interfacial instability and reduced ionic conductivity, particularly at low temperatures. This work presents a molecular engineering strategy that improves electrolyte performance through molecular coordination and physical encapsulation. An encapsulated gel polymer electrolyte (EGPE) is created by confining sodium bis(trifluoromethanesulfonyl)imide, succinonitrile (SN), and trimethyl phosphate (TMP) within a poly(vinylene carbonate) network formed via in situ polymerization. This network not only provides effective encapsulation by physically immobilizing reactive liquid components for enhanced interfacial stability but also facilitates hydrogen bonding between SN and TMP, enabling efficient ion transport. This approach yields good ionic conductivities (0.10, 0.23, and 0.78 mS cm^{-1} at −20, 0, and 40 °C), a low activation energy (0.24 eV), and stable interfacial performance, with interfacial impedance remaining stable over 30 days and 1500 h of cycling in Na|EGPE|Na symmetric cells. Na|EGPE|$Na_3V_2(PO_4)_3$ cells also show stable cycling, reaching 82.2 mAh g^{-1} after 1000 cycles at 2C (25 °C) and 99.3 mAh g^{-1} after 700 cycles at 0.2C (−10 °C).

1. Introduction

Na-ion batteries are emerging as an attractive alternative to Li-ion technology, thanks to the abundance of Na and an inherently cheaper design that supports Co-free cathodes and allows Al to replace Cu in current collectors [1–3]. Utilizing a Na-metal anode, with its low redox potential (−2.71 V vs. the standard hydrogen electrode) and high theoretical specific capacity (1166 mAh g^{-1}) [3,4], increases the energy density of Na-metal batteries (NMBs) compared to their conventional counterparts. However, significant challenges arise when the Na-metal anode interacts with conventional organic liquid electrolytes; its high reactivity can lead to ongoing electrolyte consumption and the formation of unstable solid electrolyte interphases (SEIs) [5,6]. Additionally, in NMBs, dendrite formation can occur, potentially causing performance degradation and safety hazards [5,7]. Substituting conventional liquid electrolytes with gel polymer electrolytes (GPEs) is an approach to address these issues [8,9]. However, conventional GPEs for NMBs face substantial challenges, including low ionic conductivity, interfacial instability, limited electrochemical windows, and poor cycling performance, especially at low temperatures [10,11].

Using plastic crystals, such as succinonitrile (SN), in place of conventional organic liquid solvents offers a promising path to safer electrolytes [12,13]. As a molecular plastic crystal, SN coordinates strongly with Li^+ and Na^+, enhancing salt dissociation [14]. Furthermore, as a plasticizer, it facilitates the movement of polymer chains, potentially improving ionic conductivity [15,16]. Nevertheless, the utilization of SN presents challenges. Specifically, direct contact between SN and alkali metals can catalyze the polymerization of SN, and the development of an insufficient passivation layer on the electrode surface may elevate interfacial resistance and impede electrochemical reversibility [17,18].

* Corresponding author at: Chair of Electrode Design for Electrochemical Energy Systems, University of Bayreuth, Bayreuth 95448, Bavaria, Germany.
** Corresponding authors.
E-mail addresses: dengjie.chen@jnu.edu.cn (D. Chen), francesco.ciucci@uni-bayreuth.de (F. Ciucci), jyuao@connect.ust.hk (J. Yu).
† These authors contributed equally to this work.

https://doi.org/10.1016/j.ensm.2025.104834
Received 13 October 2025; Received in revised form 16 December 2025; Accepted 21 December 2025
Available online 22 December 2025

While using a high salt concentration in electrolytes can prevent solvent reduction [19–21], this approach is often impractical due to the resulting high viscosity, which limits ionic conductivity and causes poor electrode wettability. A more effective strategy is to engineer a stable solvation shell around cations at lower concentrations by strengthening solvent-cation interactions through weak forces, such as hydrogen bonds [22]. This principle guides component selection; for instance, combining SN with ethylene carbonate (EC) utilizing hydrogen bonds creates a favorable coordination environment for Na^+ [23]. However, the flammability of organic carbonates, such as EC, poses a significant safety risk. This concern motivates substituting flammable EC with trimethyl phosphate (TMP), a flame retardant, whose methyl groups can form hydrogen bonds with SN. This choice, however, poses a critical challenge, as both unconfined TMP and SN are problematic on their own. TMP is readily reduced by alkali metals, resulting in poor compatibility and low Coulombic efficiency (CE) [24], whereas, as described above, SN can cause significant interfacial instability [25]. Therefore, the central requirement for developing a functional GPE with SN and TMP is to overcome the inherent interfacial incompatibility with Na metal. Given the larger ionic radius and higher reactivity of Na^+ compared to Li^+, a simple transplantation of classical strategies or materials is insufficient. Instead, a specific re-engineering of the intermolecular interactions is required.

To effectively address interfacial instability and suppress detrimental reactions between electrolyte constituents and the reactive Na electrode, a key strategy to address this is the creation of a stable SEI [26]. One approach involves using dual-salt electrolytes, where an anion from a second salt is preferentially reduced to form a protective SEI layer that alleviates these side reactions [21,27,28]. However, this method has a significant drawback, as it can also reduce the electrolyte's overall ionic conductivity [29]. A more common alternative is the use of a film-forming additive [30], such as vinylene carbonate (VC). VC is widely employed owing to its ability to polymerize into durable oligomers, constructing a stable SEI layer on the metal anode with high thermal stability [31]. While highly effective as an additive, VC is unsuitable as a primary electrolyte component. If extensively incorporated within the polymer matrix, the resulting poly(vinylene carbonate) (pVC) serves as the principal medium for ion conduction. However, this polymer matrix's inherent backbone rigidity severely hinders fast ion mobility, as it induces a glassy state with limited segmental motion at ambient temperature, resulting in a prohibitively low ionic conductivity on the order of 10^{-5} S cm^{-1} and consequently rendering the electrolyte impractical [32–34].

This limitation can be circumvented in a GPE design. In such a system, the polymer network functions as a structural scaffold rather than serving as the primary ion-conducting medium. Building upon this principle, we hereby present an encapsulated gel polymer electrolyte (EGPE) produced through the in situ polymerization of VC within a porous polytetrafluoroethylene (PTFE) scaffold. The resulting EGPE is composed of a flame-retardant solvent (TMP), a solid plasticizer (SN), and sodium bis(trifluoromethanesulfonyl)imide (NaTFSI), all of which are confined within a composite network. This dual-component framework is key to our design, where the PTFE scaffold provides mechanical flexibility and high fracture toughness, and concomitantly, the poly (vinylene carbonate) (pVC) network contributes to stable SEI formation, ensuring high interfacial stability. Unlike a dense polymer matrix that impose severe steric hindrance on large Na^+, the porous PTFE scaffold hosts a percolation network where SN-mediated molecular bridging pathways facilitate the rapid transport of bulky Na^+. To explicitly differentiate our work from prior arts utilizing similar raw materials, a detailed comparison of the core design principles and mechanisms is provided in **Table S1**. Benefiting from this coordination-regulated encapsulation, the EGPE exhibits exceptional properties, including good ionic conductivities (~0.59 and 0.10 mS cm^{-1} at 25 and −20 °C, respectively), non-flammability, and long-term stability during Na stripping and plating for 1500 h. Furthermore, full Na|EGPE|$Na_3V_2(PO_4)_3$ (NVP) cells demonstrate excellent cycling stability, retaining ~96.5 % of their initial capacity after 1000 cycles at 25 °C and delivering 99.3 mAh g^{-1} for 700 cycles even at –10 °C. These results provide a new perspective on the development of GPEs via polymerization-mediated coordination, offering pathways to produce high-performance NMBs in challenging operational environments.

2. Results and discussion

2.1. Electrolyte design and optimization

The preparation process of EGPE is illustrated in Fig. 1**a**. EGPE was synthesized via the in situ polymerization of a flowable precursor solution (**Figure S1a**) with a porous PTFE framework (Fig. 1**b**). The PTFE support was chosen to facilitate rapid infiltration of the precursor while providing mechanical robustness and thermal stability [35]. Following free-radical polymerization at 60 °C, the liquid transformed into a quasi-solid state (**Figure S1b**), resulting in a flat, smooth, and pore-free membrane with a thickness of ~145 μm (Fig. 1**c**) and endowed with flexibility (Fig. 1**d**). To maximize ionic conductivity, the ratios of VC, SN, and NaTFSI were systematically varied while the volume of TMP was held constant. The corresponding ionic conductivities are summarized in **Table S2** and Fig. 1**e**. The optimal formulation, with a VC:SN:NaTFSI molar ratio of 1:1:2.2, achieved the highest ionic conductivity of 0.59 mS cm^{-1} at 25 °C. This optimized EGPE also demonstrated excellent temperature-dependent performance, with conductivities of 0.10, 0.23, and 0.78 mS cm^{-1} at −20, 0, and 40 °C, respectively **(Figure S2a)**. An Arrhenius plot derived from these temperature-dependent measurements yielded a low activation energy of 0.24 eV (**Figure S2b**). These transport metrics are superior to those of many recently reported Na-based polymer electrolytes, as summarized in **Table S3**.

To elucidate the polymerization mechanism, EGPE was characterized by fourier transform infrared (FTIR) and nuclear magnetic resonance (NMR) spectroscopy. The FTIR spectrum of EGPE (Fig. 1**f**) shows that the C=O stretching bonds from 1774 cm^{-1} to 1826 cm^{-1} originating from the VC monomer remain unchanged, which could provide pathways for Na^+ conduction [36]. Crucially, the absence of the C=C stretching bond at ~1563 cm^{-1} in the EGPE spectrum confirms the successful transformation of VC into pVC [37]. This conversion is further supported by ^{1}H NMR spectroscopy (Fig. 1**g**), which reveals the disappearance of the –CH═CH– bond of VC at ~7.7 ppm and the emergence of a new signal corresponding to the polymer backbone (–CH_2–CH_2–) at ~5.4 ppm [34]. Based on peak-area analysis (**Figure S3**), the residual unreacted VC was only 0.10 %, indicating highly efficient polymerization. The ^{13}C NMR spectrum (**Figure S4**) also shows the disappearance of the –CH═CH– bond (~133.1 ppm) [34]. The resulting pVC structure serves multiple functions in the electrolyte: i) its unique structural integrity effectively encapsulates the SN and TMP solvents; ii) the small amount of residual VC can act as a film-forming additive, enhancing interfacial and cycling stability [38,39]; and iii) the polar C=O groups within the polymer chains create favorable pathways for Na^+ migration [36]. Both FTIR and NMR spectra (Fig. 1**f** and 1**g**) confirm that the SN and TMP components remained chemically intact throughout the polymerization process.

2.2. Intermolecular interactions and solvation structure

Beyond formulation and polymerization, the performance of an electrolyte is critically dependent on its solvation structure and the intermolecular interactions therein. To clarify the specific configuration within EGPE, a combination of spectroscopic analyses and theoretical calculations was used. FTIR analysis revealed shifts in the vibrational modes of the electrolyte components, indicating a change in the solvation environment (Fig. 2**a**). The characteristic peaks for the –CH_3 group in TMP (~2960 cm^{-1}) and the –C≡N group in SN (~2254 cm^{-1}) both exhibit a blueshift in EGPE. This effect is more pronounced in EGPE

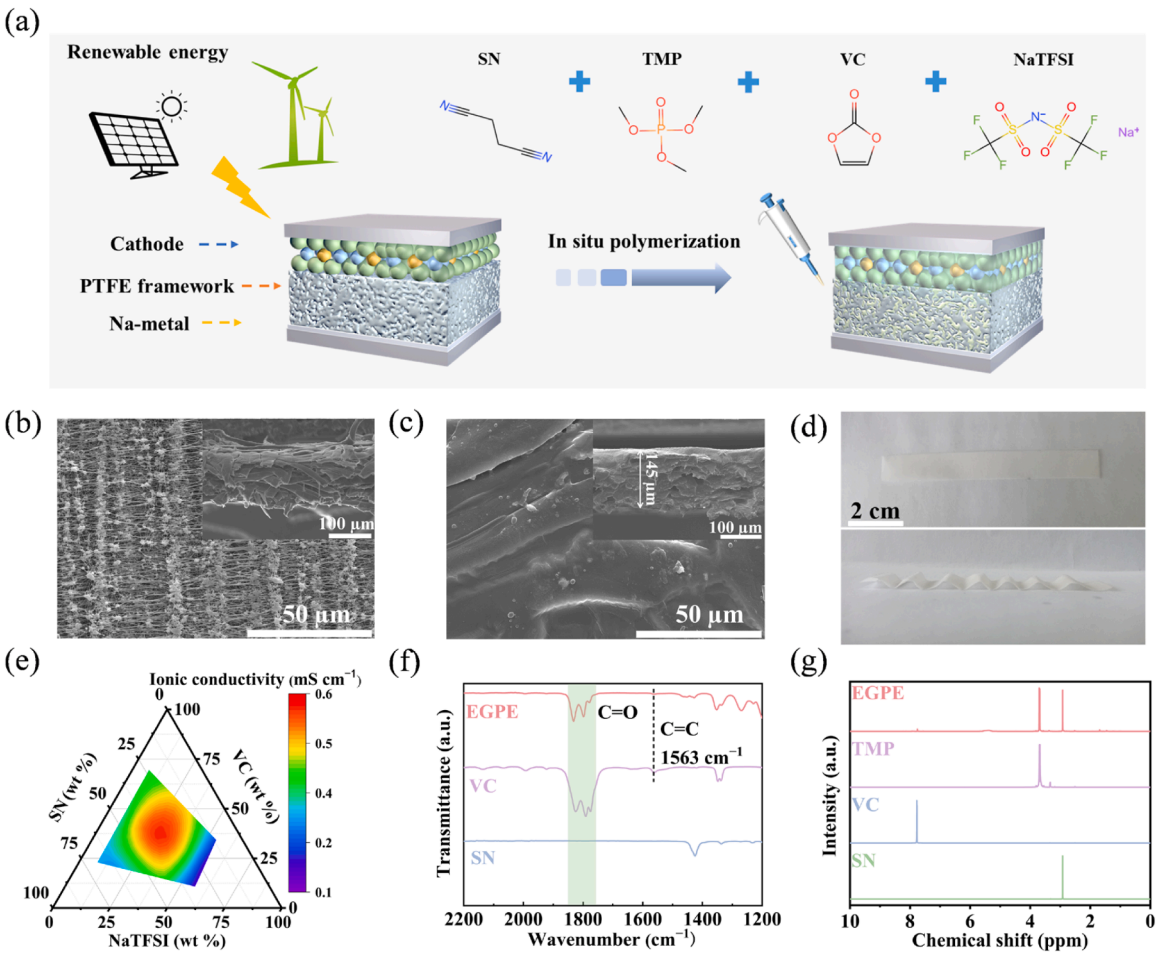

Fig. 1. Design and characterization of EGPE. (a) Schematic of the formulation strategy. Surface and cross-sectional (inset) SEM images of (b) the pristine PTFE framework and (c) the EGPE membrane. (d) Photographs of the EGPE membrane demonstrating its flexibility. (e) Ternary phase of ionic conductivity of various EGPEs at 25 °C. (f) FTIR and (g) ^{1}H NMR spectra of the constituent components and EGPE.

compared to control electrolytes lacking either SN or TMP, indicating a specific, enhanced interaction between the two solvent molecules [40, 41]. To further assess the thermodynamic stability of this coordination, variable-temperature FTIR spectroscopy was conducted from 0 to 40 °C. The characteristic vibrational peaks corresponding to the –CH_3, –C≡N, and P=O functional groups show negligible shift throughout the temperature range (**Figure S5**), demonstrating structural integrity of the TMP–SN complex. The interaction was further clarified by NMR spectroscopy. The ^{1}H NMR spectrum shows a more significant shift for the –CH_3 band of TMP in the presence of SN, confirming their interaction (**Figure S6**). Furthermore, ^{13}C NMR spectra (Fig. 2**b**) show a distinct up-field shift for both −CH_3 and −C≡N, which is characteristic of intermolecular hydrogen bond formation (C≡N···H_3C–) between SN and TMP.

Raman spectroscopy was used to correlate this interaction with electrolyte performance. As shown in Fig. 2**c**, distinct peak shifts are observed in the characteristic regions of EGPE compared to SN and TMP. Specifically, the −C≡N group of SN exhibits a clear blueshift at ~2254 cm^{-1}. Moreover, the spectral region ~740 cm^{-1}, which contains overlapping signals from the P–O–C stretching of TMP and the S–N–S symmetric stretching vibration of $TFSI^{-}$, exhibits distinct shifts in EGPE [42]. Given that TMP concentration is held constant across formulations (except for the TMP-free control), variations in this overlapping band predominantly arise from changes in $TFSI^{-}$ coordination states. Accordingly, this band was assigned to solvent-separated ion pairs (SSIPs), contact ion pairs (CIPs), and aggregates (AGGs) (**Figure S7**) [43]. As detailed in **Table S4**, the optimized EGPE achieves a high SSIP fraction of 64.10 %, significantly surpassing the control electrolytes without TMP (40.69 %) or SN (46.10 %). This quantitative evidence confirms that the TMP···SN coordination synergistically weakens the Na^{+}-$TFSI^{-}$ association.

The functional benefit of this unique solvation structure on interfacial stability was visually confirmed by contacting the electrolytes with Na metal (Fig. 2**d**). The Na metal surface remained pristine and glossy after prolonged contact with EGPE. In contrast, the Na metal surface showed significant degradation and turned a dull yellow in the TMP-free EGPE, SN-free EGPE, and SN-based liquid electrolyte (ESLE). These results demonstrate that the combination of TMP-SN interaction and polymer encapsulation is crucial for creating a stable interface with the Na-metal anode.

To validate the proposed mechanism, classical molecular dynamics (MD) and density functional theory (DFT) calculations were performed. The MD simulations provided direct evidence for hydrogen bonding, revealing that TMP and SN molecules maintain a close proximity of approximately 0.25 to 0.26 nm (Fig. 2**e**). To quantify the effect of the hydrogen bond on Na^{+} coordination, the binding energies were calculated (Fig. 2**f-h**). The binding energy between Na^{+} and the hydrogen-bonded TMP···SN complex was −0.94 eV. This value is more negative than the binding energies of Na^{+} with individual TMP (ΔE = −0.88 eV) or SN (ΔE = −0.60 eV) molecules. The robust binding energy confirms that the P=O bond acts as the primary active site for Na^{+} coordination. We further monitored the bond length of P=O. The bond length elongates from 1.4824 Å in pure TMP to 1.4869 Å in the TMP-Na^{+} system, confirming the weakening of the P=O bond character induced by the

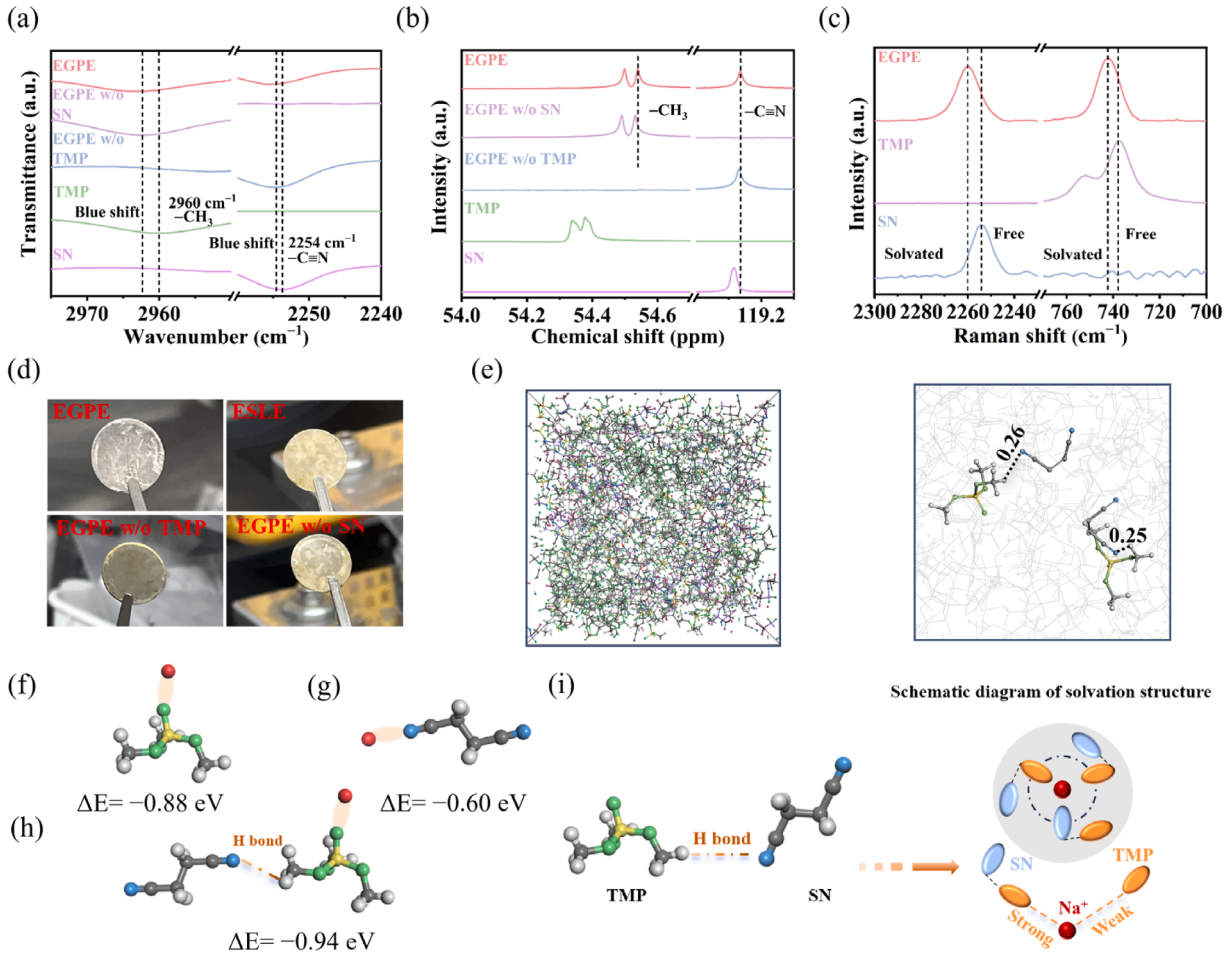

Fig. 2. The solvation structure and intermolecular interactions within EGPE. (a) FTIR, (b) ^{13}C NMR, and (c) Raman spectra comparing EGPE with its constituent components. (d) Digital photographs comparing Na-metal after contact with different electrolytes. (e) Snapshot of the MD simulation box for EGPE. DFT optimized structures and calculated binding energies for Na^+ complexed with (f) a single TMP molecule, (g) a single SN molecule, and (h) the hydrogen-bonded TMP···SN complex. (i) Schematic of the proposed solvation structure within EGPE, highlighting the hydrogen bonding between SN and TMP and the resulting coordination with Na^+.

polarization effect of the coordinated Na^+ [5,44]. Notably, in the SN···TMP-Na^+ complex, the bond length is observed to be 1.4872 Å. This sustained elongation demonstrates the introduction of SN and maintaining the critical coordination between the P=O bond and Na^+. Furthermore, the formation of the hydrogen bond network effectively stabilizes the solvation shell. This demonstrates a synergistic effect, where the hydrogen bond between the solvents creates a cooperative interaction that enhances their ability to coordinate with Na^+ (Fig. 2**i**).

Beyond hydrogen bonds, the specific coordination geometry plays a pivotal role in determining the continuity of ion transport pathways. Considering that each SN molecule possesses two –C≡N sites, we further investigated two potential coordination modes: "single-site coordination" (one SN coordinated with one TMP) and "dual-site coordination" (one SN coordinated with two TMPs). Comparative DFT calculations (**Figure S8**) reveal that the total binding energy of the dual-site complex (TMP···SN···TMP) is –0.22 eV, which is energetically more favorable than that of the single-site complex (–0.04 eV), suggesting that the dual-site mode dominates the solvation network. This preference enables SN to function as a molecular bridge, interconnecting adjacent TMP molecules to construct a continuous percolation network, thereby facilitating Na^+ transport. We should note that the experimental EGPE formulation contains an excess of SN relative to TMP. This excess not only forms a molecular bridge, but also leverages the plastic-crystalline nature of the surplus SN to facilitate ion transport [12].

2.3. Basic properties and electrochemical performance

X-ray diffraction analysis confirmed that EGPE is amorphous (**Figure S9**), which facilitates Na^+ transport. The thermal stability of EGPE and ESLE was assessed by thermogravimetric analysis. As shown in **Figure S10**, EGPE and ESLE exhibited a similar onset of weight loss at ~100 °C, which can be attributed to the volatility of TMP [24]. Furthermore, ESLE displayed a sharp mass loss profile, undergoing rapid evaporation with an ~70 % mass reduction before reaching 200 °C. In contrast, EGPE exhibited a more gradual degradation behavior, with <45 % weight loss observed across the same temperature range up to 200 °C. This behavior suggests that the pVC matrix not only encapsulates the volatile components but also controls their release rate upon heating. Furthermore, EGPE is mechanically robust, with a tensile strength of ~26 MPa (**Figure S11**). While this is slightly lower than the pristine PTFE substrate (~35 MPa), it remains higher than that of many recently reported GPEs (~10 MPa) [45,46].

Electrochemical voltage window is a key figure of merit for electrolytes. The anodic stability of EGPE was determined using LSV (**Figure S12**). At 0.01 mA cm^{-2}, EGPE exhibits an oxidation potential of 4.63 V vs. Na/Na^+, a significant improvement over the 4.29 V observed for ESLE. This enhancement suggests that EGPE is suitable for use with high-voltage cathodes.

To assess interfacial stability, Na||Na and Na||SS cells were assembled and characterized by electrochemical impedance spectroscopy

(EIS) and cyclic voltammetry (CV), respectively. The EIS data revealed a stark contrast between the two electrolytes. For the cell using the unpolymerized ESLE, the charge-transfer resistance (R_{ct}) increased progressively from 11.6 to 39.1 kΩ over 30 days (Fig. 3**a**), indicating continuous and unfavorable interfacial degradation. Conversely, the R_{ct} for the EGPE-based cell rose modestly from 8.2 to 9.5 kΩ during the initial 10 days and remained relatively stable thereafter (Fig. 3**b**), which suggests the formation of a stabilized SEI. These findings were corroborated by CV, which showed that Na stripping and plating were highly reversible with EGPE (**Figure S13a**), whereas significant side reactions were evident with ESLE (**Figure S13b**). This confirms that the in situ polymerization and encapsulation strategy effectively suppresses the decomposition of reactive liquid components, thereby enabling superior interfacial compatibility.

The practical implications of this enhanced stability were further supported by long-term galvanostatic cycling. The Na|EGPE|Na cell exhibited exceptional room-temperature durability, cycling for 1500 h at 0.1 mA cm^{-2} with a low and stable voltage of ~290 mV (Fig. 3**c**). In contrast, the Na|ESLE|Na cell short-circuited after 407 h. The preceding voltage fluctuations are attributed to parasitic reactions between the unconfined liquid electrolyte and the Na anode, resulting in an inhomogeneous SEI and uncontrolled dendrite growth. The robustness of the EGPE was further highlighted by its ability to sustain stable cycling for 600 h at an elevated current density of 0.2 mA cm^{-2} (**Figure S14**) and for 500 h at a low temperature of –10 °C (**Figure S15**).

Post-mortem analysis of the Na metal electrodes provided direct morphological evidence for the observed electrochemical performance. The electrode cycled with ESLE presented a loose, porous surface, with inhomogeneous deposition and the clear formation of dendrites over time (Fig. 3**d**). Conversely, the electrode from the EGPE cell (Fig. 3**e**) maintained a smooth and compact morphology. This direct morphological evidence confirms the unique advantage of the proposed coordination-encapsulation structure for NMBs. The in situ polymerized VC framework, combined with the robust SN-TMP percolating coordination network, effectively regulates the homogeneous flux of Na^+. This outstanding electrochemical performance, which surpasses that of many recently reported electrolytes (Fig. 3**f** and **Table S3**), is attributed to two synergistic factors. First, the combination of a regulated solvation structure and in situ polymerization suppresses side reactions between the highly reactive SN and TMP components and the anode. Second, the resulting stable interface promotes uniform Na deposition, effectively inhibiting dendrite growth and ensuring long-term cycling stability (Fig. 3**g**).

To investigate the microstructure and chemical composition of the resulting interfacial layers, Na||Na cells were disassembled after 100 cycles for detailed analysis. Post-cycling characterization of the anode surfaces immediately revealed stark morphological differences (**Figure S16**). Time-of-flight secondary ion mass spectrometry (TOF-SIMS) was further employed to probe the chemical compositions of the interface formed by Na and EGPE. The resulting 3D and 2D chemical maps show that the SEI is predominantly composed of inorganic species, including NaF_2^-, $Na_2F_3^-$, and NaO^- fragments, which are distributed throughout the layer (Fig. 4**a-b**). In contrast, organic fragments such as CF_3^- and $C_2H_3O^{\cdot-}$ were present only in low abundance. These inorganic components were also found to be distributed with high homogeneity across the interface (**Figure S17**). The formation of such a uniform, inorganic-rich SEI, particularly one with a high concentration of NaF, is known to be highly beneficial for stable cycling. It effectively suppresses dendrite formation and facilitates uniform ion transport, thereby enhancing interfacial stability [47–49].

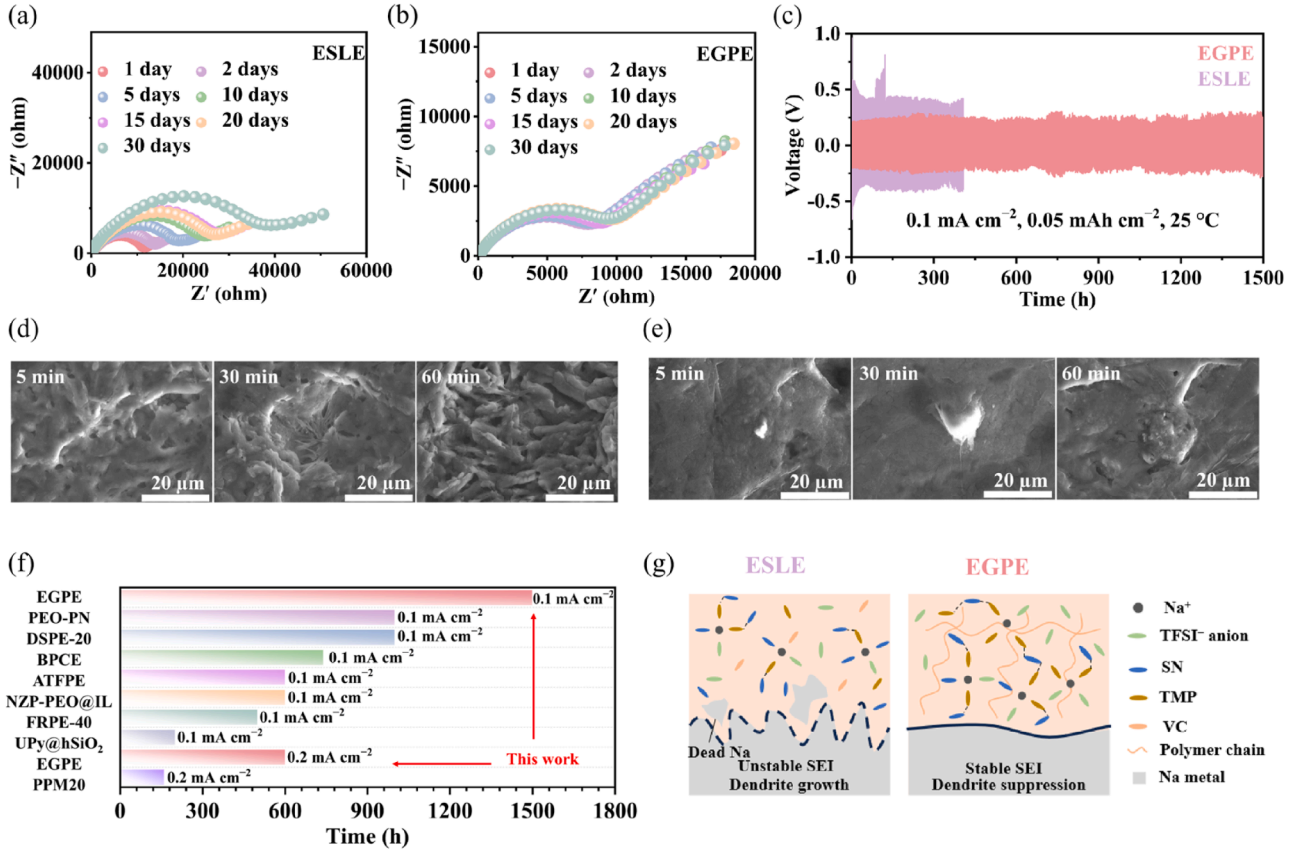

Fig. 3. Electrochemical performance of the Na||Na cells with EGPE. EIS of the (a) Na|ESLE|Na and (b) Na|EGPE|Na symmetric cells with the elapsed days. (c) Na stripping and plating profiles of the Na|EGPE|Na symmetrical cell. SEM images of the cells with (d) ESLE and (e) EGPE from 5 to 60 min. (f) Comparison of stripping and plating performance of the Na|EGPE|Na cell with recently published works. (g) A possible mechanism governs the high stability of EGPE.

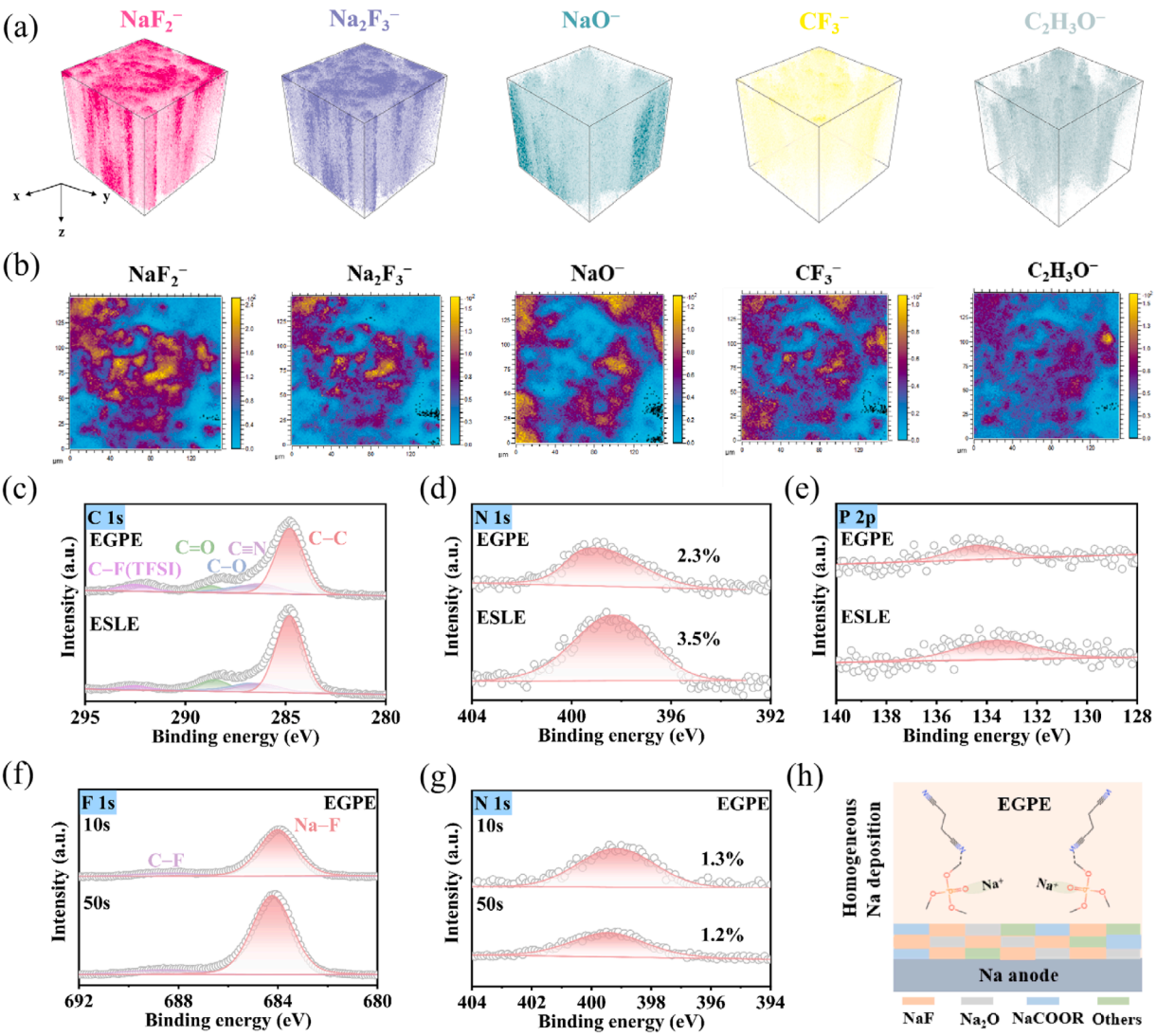

Fig. 4. Chemical composition and structure of the SEI on the Na-metal anode. (a) 3D and (b) 2D TOF-SIMS chemical maps showing the distribution of various fragment ions on the Na electrode from a cycled Na|EGPE|Na cell. High-resolution XPS spectra comparing the surface composition of the SEI formed using EGPE versus ESLE for the (c) C 1s, (d) N 1s, and (e) P 2p. In-depth XPS spectra of the (f) F 1s and (g) N 1s regions for the SEI formed using EGPE. (h) Schematic of the proposed composition and layered structure of the SEI formed on the Na-metal anode with the EGPE.

To further characterize the chemical composition of the SEI layers, X-ray photoelectron spectroscopy (XPS) was conducted on the cycled Na-metal electrodes. The survey spectra confirmed that the surfaces are primarily composed of carbon, oxygen, and fluorine (**Figure S18**). Detailed analysis of the high-resolution F 1s spectra (**Figure S19**) reveals that the SEI layer is dominated by species assigned to NaF (683.7 eV) and C–F (688.8 eV) [36], with NaF likely resulting from the decomposition of the NaTFSI salt. Significantly, the relative content of beneficial, inorganic NaF is much higher in the SEI layer formed with EGPE compared to that formed with ESLE. The C 1s spectra (Fig. 4**c**) show the presence of C–F bonds (~292.5 eV) [36], along with other characteristic peaks corresponding to C–C (~284.8 eV), C≡N (~286.3 eV), C–O (~286.7 eV), and C=O (~288.7 eV) [50,51]. The O 1s spectra (**Figure S20**) exhibit characteristic peaks for Na_2O (~529.8 eV), C=O (~531.2 eV), C–O (~532.3 eV), and a Na-Auger signal (~535.5 eV) [52, 53]. Notably, the relative ratio of organic C–O species is lower in the SEI from EGPE than that in ESLE, whereas the C=O signal becomes more prominent. This reduction in C–O species is attributed to the encapsulation effect of the in situ polymerized VC, which limits direct contact between the liquid components and the anode. The distinct differences in the N 1s spectra (Fig. 4**d**) and the suppressed P 2p spectra (Fig. 4**e**) further support this conclusion, indicating that the combined effects of encapsulation and the unique solvation structure in EGPE effectively suppress the decomposition of its core components.

XPS depth profiling was performed using Ar^+ sputtering to characterize the SEI structure. The depth profile reveals a compositional gradient within the SEI formed with EGPE. As sputtering progressed from the surface (0 s) into the inner layer (10 and 50 s), the overall atomic concentrations of C, O, and N decreased, indicating that organic species are concentrated at the outer surface (**Figure S21**). This layered structure was confirmed by high-resolution spectra of the individual elements. F 1s spectra analysis revealed that surface C–F bonds were progressively replaced by NaF, which was the dominant fluorine-containing species in the bulk of the SEI (Fig. 4**f**). Similarly, the characteristic peak for Na_2O in the O 1s spectra decreased in intensity with increasing depth, suggesting that Na_2O was an outer-layer component of the SEI (**Figure S22**). The peak intensity and atomic percentage (from 1.3 % to 1.2 %) of N 1s remained low throughout the etching process (Fig. 4**g**), confirming that SN decomposition was minimal. Furthermore, the atomic concentration of phosphorus detected within the SEI was negligible (~0.3 %) (**Figure S23**), which provides strong evidence that the degradation of TMP was suppressed. Fig. 4**h** illustrates a schematic

of the proposed composition and layered structure of the SEI formed on the Na-metal anode with EGPE, where robust, electronically insulating species are critical for creating a stable interphase.

To assess its practical viability, the EGPE was evaluated in Na||NVP full cells. At 25 °C and 0.5C, the Na|EGPE|NVP cell delivered an initial discharge capacity of ~96.4 mAh g^{-1} and showed excellent cycling stability, retaining a capacity of ~92.3 mAh g^{-1} with a CE of >99 % after 480 cycles (Fig. 5**a**). In contrast, the cell using the unpolymerized ESLE failed rapidly; its discharge capacity plummeted after 110 cycles and dropped below 6.1 mAh g^{-1} within 120 cycles. This poor performance was attributed to side reactions at the anode, which was consistent with the high and unstable polarization voltage (>0.4 V) of the ESLE cell compared to the stable ~0.2 V hysteresis of the EGPE cell (**Figure S24**). Furthermore, the Na|EGPE|NVP cell exhibited superior rate capability, delivering higher discharge capacities of 102.8 mAh g^{-1} (0.2C), 101.5 mAh g^{-1} (0.5C), 97.1 mAh g^{-1} (1C), and 82.4 mAh g^{-1} (2C), respectively (**Figure S25 and S26**). The robustness of EGPE was further demonstrated under more demanding conditions. When cycled at a high rate of 2C, the Na|EGPE|NVP cell maintained a capacity retentain of ~96.5 % and a discharge capacity of 82.2 mAh g^{-1} after 1000 cycles, with a CE above 99.6 % (Fig. 5**b**). The electrolyte also proved highly effective at low temperatures; at –10 °C and 0.2C, the Na|EGPE|NVP cell delivered a discharge capacity of 99.3 mAh g^{-1} with a CE above 99.9 % for over 700 cycles (Fig. 5**c**). This outstanding performance is mechanistically supported by MD simulations conducted at low temperature (**Figure S27**). As shown in Fig. 5**d**, the corresponding Na^+ diffusion coefficient (D_{Na^+}) remains a high level of 3.22 × 10^{-9} cm^2 s^{-1} at −20 °C, a magnitude comparable to ion transport in liquid-state environments [54]. Crucially, the radial distribution function (RDF) analysis (Fig. 5**e**) reveals that Na^+ is preferentially solvated by the oxygen atoms of TMP (Na-O_{TMP}) rather than the polymer matrix. This specific coordination environment implies that at such low temperatures, the TMP-dominated solvation shell remains active. The observation is consistent with the DFT results that the SN-mediated hydrogen bond network bridges neighboring TMP molecules to facilitate ion transport.

Based on its wide electrochemical stability window, the EGPE's performance at high voltages was also investigated. As shown in Fig. 5**f**, the EGPE-based cell maintained a negligible and low leakage current at applied voltages up to 4.5 V. In stark contrast, the ESLE-based cell exhibited rapid current runaway, indicating severe electrolyte decomposition at high potentials. This stability enabled an Na|EGPE|NVP cell to be cycled in an extended voltage window of 2.0–4.5 V (Fig. 5**g** and 5**h**). The cell delivered exceptional performance, retaining 99.0 % of its capacity after 120 cycles with a stable CE greater than 99.2 %. Collectively, these results confirm that the synergistic effects of encapsulation and coordination enable the EGPE to operate with outstanding stability across a wide range of conditions, including high operating voltages and both ambient and low temperatures.

The cycling stability of the Na|EGPE|NVP cell was also critically dependent on the formation of a stable cathode electrolyte interlayer (CEI) on the NVP cathode. Transmission electron microscopy (TEM) analysis revealed stark differences in the CEI morphology. Compared to the pristine NVP surface (Fig. 6**a**), the cathode cycled with ESLE formed a non-uniform and incomplete CEI layer (Fig. 6**b**). In contrast, cycling with EGPE resulted in a dense, well-connected, and uniform CEI of ~8.5

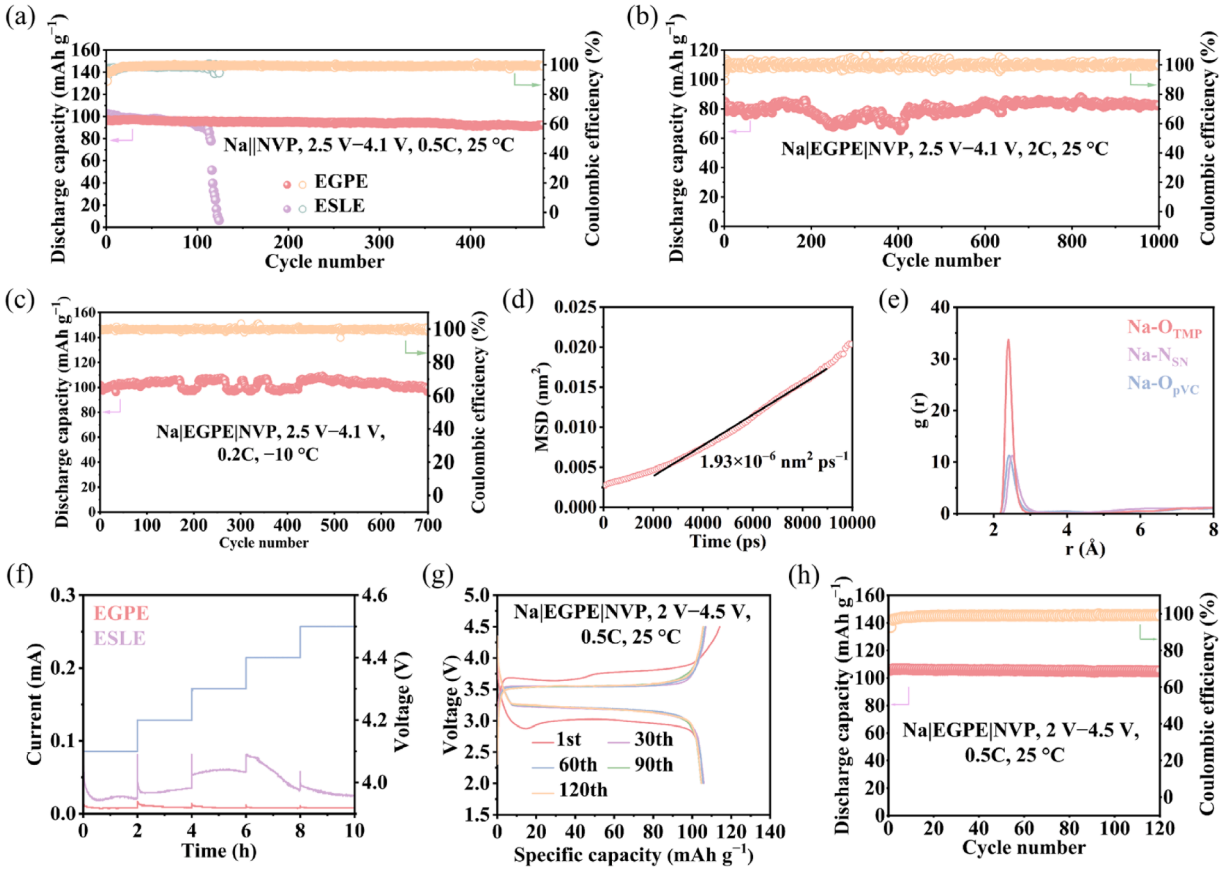

Fig. 5. Electrochemical performance of the Na||NVP full cells with EGPE. (a) Comparative cycling performance and CE of Na||NVP cells using either EGPE or ESLE at 25 °C and 0.5C (1C = 117 mA g^{-1}). (b) Long-term cycling stability of the Na|EGPE|NVP cell at 25 °C and 2C. (c) Low-temperature cycling performance of the Na|EGPE|NVP cell at −10 °C and 0.2C. (d) The calculated MSD of Na^+ in EGPE at −20 °C. (e) Radial distribution function g(r) with reference to Na^+ in EGPE at −20 °C. (f) Electrochemical floating test comparing the leakage current of EGPE and ESLE-based cells at sequentially increasing voltages up to 4.5 V. (g) Charge and discharge profiles and (h) corresponding long-term cycling stability of the Na|EGPE|NVP cell operated in an extended voltage window of 2.0 V to 4.5 V.

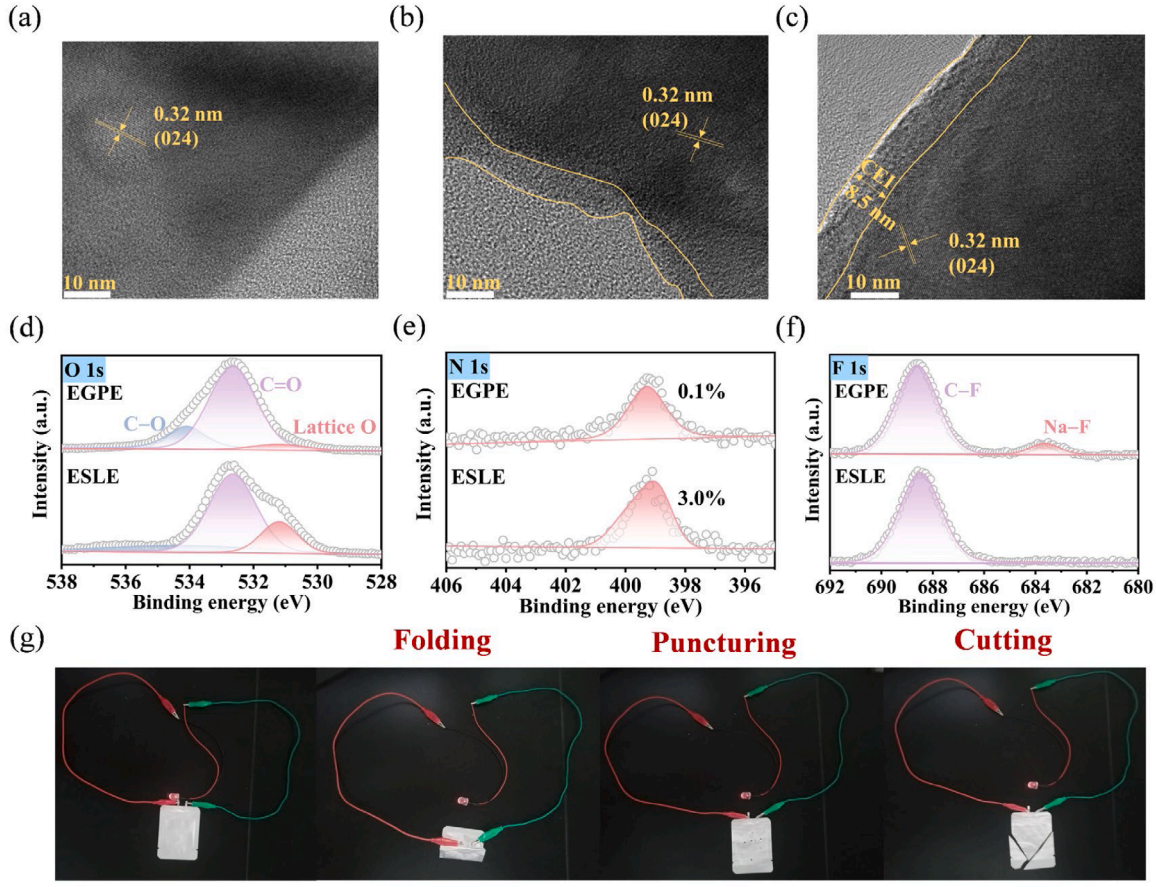

Fig. 6. TEM images of (a) the pristine and cycled NVP cathodes with (b) ESLE and (c) EGPE. (d) O 1s, (e) N 1s, and (f) F 1s of the CEI layer on the cycled NVP cathode with ESLE and EGPE. (g) Safety evaluation of the Na|EGPE|NVP pouch cell under destructive conditions.

nm thick (Fig. 6**c**). This indicated superior interfacial compatibility between the cathode and EGPE. XPS was used to further probe the chemical composition of this interphase. The O 1s spectra indicate that the CEI formed with ESLE exhibited a significantly higher intensity for the lattice oxygen peak (~531.2 eV) compared to the CEI from the EGPE system (Fig. 6**d**). This suggested that the non-uniform layer in the ESLE system exposed parts of the NVP active material directly to the electrolyte. The N 1s spectra (Fig. 6**e**) show lower peak intensity and atomic percentage in the EGPE system, confirming that the decomposition of SN was effectively suppressed at the cathode surface. The F 1s spectra in both systems display a prominent C-F peak (~688.8 eV), originating from the PVDF binder in the cathode. Notably, the cell utilizing EGPE exhibits a distinct Na-F peak (~683.7 eV), where NaF is crucial for forming a more stable and robust CEI (Fig. 6**f**).

The flammability of the EGPE was evaluated through direct flammability tests against control materials. As shown in **Figure S28a** and **Video S1**, a commercial polypropylene (PP) separator proved highly flammable, igniting immediately and burning out completely upon exposure to a flame. An EGPE formulated without TMP also eventually burned under continuous ignition, though it showed a slight retarding effect from SN (**Figure S28b and Video S2**). In stark contrast, the complete EGPE demonstrated exceptional fire resistance, failing to ignite and retaining its original appearance even after prolonged and direct contact with a flame (**Figure S28c and Video S3**). Beyond its inherent non-flammability, the practical safety and mechanical robustness of EGPE were confirmed using a pouch cell. An Na|EGPE|NVP pouch cell successfully powered a light-emitting diode without failure, even while being subjected to severe physical abuse such as being folded, punctured, and cut (Fig. 6**g**). This remarkable resilience under destructive conditions underscores the excellent safety and practicality of EGPE for demanding battery applications.

3. Conclusions

In this work, we have designed EGPEs that enable durable, safe, and high-performance NMBs capable of robust operation under both ambient and low-temperature conditions. The success of this electrolyte is attributed to a multi-scale encapsulation strategy that combines physical confinement via a porous PTFE-reinforced in situ polymerization network with engineered intermolecular interactions. Specifically, the polymerization of VC creates a robust framework that encapsulates the liquid components while simultaneously forming a stable SEI. Concurrently, hydrogen bonding between SN and TMP fosters the formation of a TMP···SN complex where SN functions as a molecular bridge to interconnect neighboring TMP molecules that primarily coordinate with Na^+. This unique solvation structure not only promotes high ionic conductivity (~0.59 and ~0.10 mS cm^{-1} at 25 and −20 °C, respectively) but also crucially passivates the reactive SN against the Na-metal anode. This multi-faceted design directly translates into exceptional electrochemical performance. Na||NVP full cells exhibit outstanding long-term cycling stability, with a capacity retention of ~96.5 % after 1000 cycles at 2C and 25 °C, and a superior ~99.9 % retention after 700 cycles at 0.2C and −10 °C. The resulting cells exhibit exceptional robustness, maintaining stable cycling across a wide 2.0–4.5 V window while also demonstrating significantly enhanced safety in pouch cell ignition. This work demonstrates that a synergistic strategy, which intelligently combines in situ polymerization-enabled encapsulation with engineered intermolecular interactions, is a novel pathway toward highly compatible and safe electrolytes for next-generation NMBs.

CRediT authorship contribution statement

Junhao Chen: Writing – original draft, Visualization, Methodology, Investigation. **Wentao Lin:** Writing – original draft, Validation, Investigation. **Zhantao Wu:** Software. **Dengjie Chen:** Writing – review & editing, Supervision, Resources, Conceptualization. **Ho Mei Law:** Writing – review & editing. **Francesco Ciucci:** Writing – review & editing, Software, Resources. **Jing Yu:** Writing – review & editing, Supervision, Funding acquisition, Conceptualization.

Declaration of competing interest

The authors declare that they have no known competing financial interests or personal relationships that could have appeared to influence the work reported in this paper.

Acknowledgements

This study was supported by the Guangdong Basic and Applied Basic Research Foundation (No. 2024A1515010292). FC would like to thank the University of Bayreuth and the Bavarian Center for Battery Technology (BayBatt) for providing start-up funds. The authors also gratefully acknowledge Dr. Zilong Wang from the Hong Kong University of Science and Technology for his technical guidance on the DFT calculations. During the preparation of this manuscript, the authors used Gemini (Google) to improve the language and clarity of certain parts. After using these tools, the authors reviewed and edited the content as needed and take full responsibility for the content of the published article.

Supplementary materials

Supplementary material associated with this article can be found, in the online version, at doi:10.1016/j.ensm.2025.104834.

Data availability

Data will be made available on request.

References

[1] C. Vaalma, D. Buchholz, M. Weil, S. Passerini, A cost and resource analysis of sodium-ion batteries, Nat. Rev. Mater. 3 (2018) 18013, https://doi.org/10.1038/natrevmats.2018.13.
[2] V. Palomares, M. Casas-Cabanas, E. Castillo-Martínez, M.H. Han, T. Rojo, Update on Na-based battery materials. A growing research path, Energy Environ. Sci. 6 (2013) 2312–2337, https://doi.org/10.1039/C3EE41031E.
[3] H. Wang, D. Yu, C. Kuang, L. Cheng, W. Li, X. Feng, Z. Zhang, X. Zhang, Y. Zhang, Alkali metal anodes for rechargeable batteries, Chem 5 (2019) 313–338, https://doi.org/10.1016/j.chempr.2018.11.005.
[4] X. Xia, C.-F. Du, S. Zhong, Y. Jiang, H. Yu, W. Sun, H. Pan, X. Rui, Y. Yu, Homogeneous Na deposition enabling high-energy Na-metal batteries, Adv. Funct. Mater. 32 (2022) 2110280, https://doi.org/10.1002/adfm.202110280.
[5] J. Wang, Y. Yamada, K. Sodeyama, E. Watanabe, K. Takada, Y. Tateyama, A. Yamada, Fire-extinguishing organic electrolytes for safe batteries, Nat. Energy 3 (2018) 22–29, https://doi.org/10.1038/s41560-017-0033-8.
[6] P. Jaumaux, J. Wu, D. Shanmukaraj, Y. Wang, D. Zhou, B. Sun, F. Kang, B. Li, M. Armand, G. Wang, Non-flammable liquid and quasi-solid electrolytes toward highly-safe alkali metal-based batteries, Adv. Funct. Mater. 31 (2021) 2008644, https://doi.org/10.1002/adfm.202008644.
[7] L. Kong, Y. Li, W. Feng, Strategies to solve lithium battery thermal runaway: from mechanism to modification, Electrochem. Energy Rev. 4 (2021) 633–679, https://doi.org/10.1007/s41918-021-00109-3.
[8] F. Gebert, J. Knott, R. Gorkin, S.-L. Chou, S.-X. Dou, Polymer electrolytes for sodium-ion batteries, Energy Storage Mater. 36 (2021) 10–30, https://doi.org/10.1016/j.ensm.2020.11.030.
[9] J. Pan, N. Wang, H.J. Fan, Gel polymer electrolytes design for Na-ion batteries, Small Methods 6 (2022) 2201032, https://doi.org/10.1002/smtd.202201032.
[10] F. Wu, K. Zhang, Y. Liu, H. Gao, Y. Bai, X. Wang, C. Wu, Polymer electrolytes and interfaces toward solid-state batteries: recent advances and prospects, Energy Storage Mater. 33 (2020) 26–54, https://doi.org/10.1016/j.ensm.2020.08.002.
[11] J. Yu, Y. Wang, L. Shen, J. Liu, Z. Wang, S. Xu, H.M. Law, F. Ciucci, Fast-charging solid-state Li batteries: materials, strategies, and prospects, Adv. Mater. 37 (2025) 2417796, https://doi.org/10.1002/adma.202417796.
[12] P.-J. Alarco, Y. Abu-Lebdeh, A. Abouimrane, M. Armand, The plastic-crystalline phase of succinonitrile as a universal matrix for solid-state ionic conductors, Nat. Mater. 3 (2004) 476–481, https://doi.org/10.1038/nmat1158.
[13] X. Ye, H. Fu, Y. Zhang, D. Wu, Y. Zhong, X. Wang, X. Ouyang, J. Tu, Modulating the Li-ion transport pathway of succinonitrile-based plastic crystalline electrolytes for solid-state lithium metal batteries, Adv. Funct. Mater. 35 (2025) 2413205, https://doi.org/10.1002/adfm.202413205.
[14] M. Liao, Y. Zhou, X. Jiang, R. Wan, In situ construction of 3D Li channels high-temperature-resistant polymer electrolyte and Li_3N-rich interface enabling stable solid-state Li metal battery, Chem. Eng. J. 480 (2024) 148020, https://doi.org/10.1016/j.cej.2023.148020.
[15] X. Pei, Y. Li, T. Ou, X. Liang, Y. Yang, E. Jia, Y. Tan, S. Guo, Li−N interaction induced deep eutectic gel polymer electrolyte for high performance lithium-metal batteries, Angew. Chem. Int. Ed. 61 (2022) e202205075, https://doi.org/10.1002/anie.202205075.
[16] L.-Z. Fan, Y.-S. Hu, A.J. Bhattacharyya, J. Maier, Succinonitrile as a versatile additive for polymer electrolytes, Adv. Funct. Mater. 17 (2007) 2800–2807, https://doi.org/10.1002/adfm.200601070.
[17] D. Zhang, Y. Liu, Z. Sun, Z. Liu, X. Xu, L. Xi, S. Ji, M. Zhu, J. Liu, Eutectic-based polymer electrolyte with the enhanced lithium salt dissociation for high-performance lithium metal batteries, Angew. Chem. Int. Ed. 62 (2023) e202310006, https://doi.org/10.1002/anie.202310006.
[18] C. Wu, W. Zeng, Gel electrolyte for Li metal battery, Chem. Asian J. 17 (2022) e202200816, https://doi.org/10.1002/asia.202200816.
[19] K. Takada, Y. Yamada, E. Watanabe, J. Wang, K. Sodeyama, Y. Tateyama, K. Hirata, T. Kawase, A. Yamada, Unusual passivation ability of superconcentrated electrolytes toward hard carbon negative electrodes in sodium-ion batteries, ACS Appl. Mater. 9 (2017) 33802–33809. https://pubs.acs.org/doi/10.1021/acsami.7b08414.
[20] Y. Li, Z. Wang, W. Lin, B. Wei, D. Chen, A concentrated electrolyte of LiTFSI and dimethyl carbonate for high-voltage Li batteries, ACS Appl. Energy Mater. 6 (2023) 9337–9346. https://pubs.acs.org/doi/10.1021/acsaem.3c01206.
[21] W. Lin, D. Chen, J. Yu, Manipulating the ionic conductivity and interfacial compatibility of polymer-in-dual-salt electrolytes enables extended-temperature quasi-solid metal batteries, J. Colloid Interface Sci. 666 (2024) 189–200, https://doi.org/10.1016/j.jcis.2024.04.026.
[22] J. Zhang, Y. Zhang, J. Fu, X. Li, C. Zhang, Perspective on eutectic electrolytes for next-generation batteries, Electron 2 (2024) e57, https://doi.org/10.1002/elt2.57.
[23] M. Jiang, T. Li, Y. Qiu, X. Hou, H. Lin, Q. Zheng, X. Li, Electrolyte design with dual –C≡N groups containing additives to enable high-voltage $Na_3V_2(PO_4)_2F_3$-based sodium-ion batteries, J. Am. Chem. Soc. 146 (2024) 12519–12529, https://doi.org/10.1021/jacs.4c00702.
[24] J. Yu, Y.-Q. Lyu, J. Liu, M.B. Effat, S.C.T. Kwok, J. Wu, F. Ciucci, Enabling non-flammable Li-metal batteries via electrolyte functionalization and interface engineering, J. Mater. Chem. A 7 (2019) 17995–18002, https://doi.org/10.1039/C9TA03784E.
[25] S. Zhang, S. Li, Y. Lu, Designing safer lithium-based batteries with nonflammable electrolytes: a review, eScience 1 (2021) 163–177, https://doi.org/10.1016/j.esci.2021.12.003.
[26] W. Liu, P. Liu, D. Mitlin, Review of emerging concepts in SEI analysis and artificial SEI membranes for lithium, sodium, and potassium metal battery anodes, Adv. Energy Mater. 10 (2020) 2002297, https://doi.org/10.1002/aenm.202002297.
[27] H.M. Law, J. Yu, S.C.T. Kwok, G. Zhou, M.J. Robson, J. Wu, F. Ciucci, A hybrid dual-salt polymer electrolyte for sodium metal batteries with stable room temperature cycling performance, Energy Storage Mater. 46 (2022) 182–191, https://doi.org/10.1016/j.ensm.2022.01.001.
[28] J. Yu, J. Liu, X. Lin, H.M. Law, G. Zhou, S.C.T. Kwok, M.J. Robson, J. Wu, F. Ciucci, A solid-like dual-salt polymer electrolyte for Li-metal batteries capable of stable operation over an extended temperature range, Energy Storage Mater. 37 (2021) 609–618, https://doi.org/10.1016/j.ensm.2021.02.045.
[29] M. Cui, Y. Qin, Z. Li, H. Zhao, L. Liu, Z. Jiang, Z. Cao, J. Zhao, B. Mao, W. Yu, Y. Su, R. Vasant Kumar, S. Ding, Z. Qu, K. Xi, Retarding anion migration for alleviating concentration polarization towards stable polymer lithium-metal batteries, Sci. Bull. 69 (2024) 1706–1715, https://doi.org/10.1016/j.scib.2024.03.048.
[30] H. Wu, H. Jia, C. Wang, J.-G. Zhang, W. Xu, Recent progress in understanding solid electrolyte interphase on lithium metal anodes, Adv. Energy Mater. 11 (2021) 2003092, https://doi.org/10.1002/aenm.202003092.
[31] Z. Peng, X. Cao, P. Gao, H. Jia, X. Ren, S. Roy, Z. Li, Y. Zhu, W. Xie, D. Liu, Q. Li, D. Wang, W. Xu, J.-G. Zhang, High-power lithium metal batteries enabled by high-concentration acetonitrile-based electrolytes with vinylene carbonate additive, Adv. Funct. Mater. 30 (2020) 2001285, https://doi.org/10.1002/adfm.202001285.
[32] S. Chen, H. Che, F. Feng, J. Liao, H. Wang, Y. Yin, Z.-F. Ma, Poly(vinylene carbonate)-based composite polymer electrolyte with enhanced interfacial stability to realize high-performance room-temperature solid-state sodium batteries, ACS Appl. Mater. 11 (2019) 43056–43065, https://doi.org/10.1021/acsami.9b11259.
[33] Y. Zhao, Y. Bai, W. Li, M. An, Y. Bai, G. Chen, Design strategies for polymer electrolytes with ether and carbonate groups for solid-state lithium metal batteries, Chem. Mater. 32 (2020) 6811–6830, https://doi.org/10.1021/acs.chemmater.9b04521.
[34] J. Chai, Z. Liu, J. Ma, J. Wang, X. Liu, H. Liu, J. Zhang, G. Cui, L. Chen, In situ generation of poly (vinylene carbonate) based solid electrolyte with interfacial

stability for $LiCoO_2$ lithium batteries, Adv. Sci. 4 (2017) 1600377, https://doi.org/10.1002/advs.201600377.
[35] T. Jiang, P. He, G. Wang, Y. Shen, C.-W. Nan, L.-Z. Fan, Solvent-free synthesis of thin, flexible, nonflammable garnet-based composite solid electrolyte for all-solid-state lithium batteries, Adv. Energy Mater. 10 (2020) 1903376, https://doi.org/10.1002/aenm.201903376.
[36] Y. Li, B. Wei, J. Yu, D. Chen, Multiple Na^+ transport pathways and interfacial compatibility enable high-capacity, room-temperature quasi-solid sodium batteries, J. Colloid Interface Sci. 666 (2024) 447–456, https://doi.org/10.1016/j.jcis.2024.04.047.
[37] Y. Liu, D. Zhang, L. Luo, Z. Li, H. Lin, J. Liu, Y. Zhao, R. Hu, M. Zhu, Percolating coordinated ion transport cells in polymer electrolytes to realize room-temperature solid-state lithium metal batteries, Energy Storage Mater. 70 (2024) 103548, https://doi.org/10.1016/j.ensm.2024.103548.
[38] L. El Ouatani, R. Dedryvère, C. Siret, P. Biensan, S. Reynaud, P. Iratçabal, D. Gonbeau, The effect of vinylene carbonate additive on surface film formation on both electrodes in Li-ion batteries, J. Electrochem. Soc. 156 (2009) A103–A113, https://doi.org/10.1149/1.3029674.
[39] H. Zhao, X. Yu, J. Li, B. Li, H. Shao, L. Li, Y. Deng, Film-forming electrolyte additives for rechargeable lithium-ion batteries: progress and outlook, J. Mater. Chem. A 7 (2019) 8700–8722, https://doi.org/10.1039/C9TA00126C.
[40] T. Dobbelaere, A.K. Roy, P. Vereecken, C. Detavernier, Atomic layer deposition of aluminum phosphate based on the plasma polymerization of trimethyl phosphate, Chem. Mater. 26 (2014) 6863–6871, https://doi.org/10.1021/cm503587w.
[41] D.-M. Zhu, F. Bai, Y.-N. Zhang, Y.-N. Yang, Z. Sun, J.-W. Deng, T. Zhang, A solid-state lithium-oxygen battery operating at ambient temperature and full charge-discharge, J. Energy Storage 56 (2022) 105790, https://doi.org/10.1016/j.est.2022.105790.
[42] H. Liang, F. Yang, Z. Wu, J. Chen, R. Hu, X. Tang, L. Yang, Y. Liang, S. Li, J. Li, D. Chen, J. Yu, Solvation-regulated flame-retardant hybrid solid-like electrolytes enabling high-rate and wide-temperature sodium batteries, Compos. Part B Eng. 311 (2026) 113215, https://doi.org/10.1016/j.compositesb.2025.113215.
[43] X. Li, T. Zhang, Y. Zhao, X. Zhu, A. Ge, K.C. Gordon, F. Wang, G. Xu, M. Zhu, Enhancing robustness and charge transfer kinetics of sodium-ion batteries through introduction of anionic anchoring separators, J. Am. Chem. Soc. 147 (2025) 8488–8499, https://doi.org/10.1021/jacs.4c16227.
[44] Z. Zhou, R. Wei, X. Zhou, Y. Liu, D. Zhang, Y.-H. Lin, Chemical bonding engineering: insights into physicochemical performance optimization for energy-storage/conversion, Acc. Mater. Res. 5 (2024) 1571–1582, https://doi.org/10.1021/accountsmr.4c00243.
[45] D. Chen, M. Zhu, P. Kang, T. Zhu, H. Yuan, J. Lan, X. Yang, G. Sui, Self-enhancing gel polymer electrolyte by in situ construction for enabling safe lithium metal battery, Adv. Sci. 9 (2022) 2103663, https://doi.org/10.1002/advs.202103663.
[46] X. Cheng, J. Pan, Y. Zhao, M. Liao, H. Peng, Gel polymer electrolytes for electrochemical energy storage, Adv. Energy Mater. 8 (2018) 1702184, https://doi.org/10.1002/aenm.201702184.
[47] C. Zhu, D. Wu, Z. Wang, H. Wang, J. Liu, K. Guo, Q. Liu, J. Ma, Optimizing NaF-rich solid electrolyte interphase for stabilizing sodium metal batteries by electrolyte additive, Adv. Funct. Mater. 34 (2024) 2214195, https://doi.org/10.1002/adfm.202214195.
[48] E. Wang, J. Wan, Y.-J. Guo, Q. Zhang, W.-H. He, C.-H. Zhang, W.-P. Chen, H.-J. Yan, D.-J. Xue, T. Fang, F. Wang, R. Wen, S. Xin, Y.-X. Yin, Y.-G. Guo, Mitigating electron leakage of solid electrolyte interface for stable sodium-ion batteries, Angew. Chem. Int. Ed. 62 (2023) e202216354, https://doi.org/10.1002/anie.202216354.
[49] H. Wang, C. Zhu, J. Liu, S. Qi, M. Wu, J. Huang, D. Wu, J. Ma, Formation of NaF-rich solid electrolyte interphase on Na anode through additive-induced anion-enriched structure of Na^+ solvation, Angew. Chem. Int. Ed. 61 (2022) e202208506, https://doi.org/10.1002/anie.202208506.
[50] S. Ma, Y. Zhang, D. Zhang, Y. Zhang, W. Li, K. Ji, Z. Tang, M. Chen, –C≡N functionalizing polycarbonate-based solid-state polymer electrolyte compatible to high-voltage cathodes, J. Energy Chem. 98 (2024) 422–431, https://doi.org/10.1016/j.jechem.2024.06.052.
[51] Y. Lu, Y. Cai, Q. Zhang, L. Liu, Z. Niu, J. Chen, A compatible anode/succinonitrile-based electrolyte interface in all-solid-state Na–CO_2 batteries, Chem. Sci. 10 (2019) 4306–4312, https://doi.org/10.1039/C8SC05178J.
[52] P. Liu, L. Miao, Z. Sun, X. Chen, Y. Si, Q. Wang, L. Jiao, Inorganic–organic hybrid multifunctional solid electrolyte interphase layers for dendrite-free sodium metal anodes, Angew. Chem. Int. Ed. 62 (2023) e202312413, https://doi.org/10.1002/anie.202312413.
[53] J. Zheng, J. Zhang, W. Li, J. Ge, W. Chen, Phosphate-based gel polymer electrolyte enabling remarkably long cycling stable sodium storage in a wide-operating-temperature, Chem. Eng. J. 465 (2023) 142796, https://doi.org/10.1016/j.cej.2023.142796.
[54] J. Yu, X. Lin, J. Liu, J.T.T. Yu, M.J. Robson, G. Zhou, H.M. Law, H. Wang, B. Z. Tang, F. Ciucci, In situ fabricated quasi-solid polymer electrolyte for high-energy-density lithium metal battery capable of subzero operation, Adv. Energy Mater. 12 (2022) 2102932, https://doi.org/10.1002/aenm.202102932.